Is disrupted nucleotide-substrate cooperativity a common trait for Cushing's syndrome driving mutations of protein kinase A?

Walker, Caitlin; Wang, Yingjie; Olivieri, Cristina; V.S, Manu; Gao, Jiali; Bernlohr, David A.; Calebiro, Davide; Taylor, Susan S.; Veglia, Gianluigi

Document Version
Peer reviewed version

Citation for published version (Harvard):
Walker, C, Wang, Y, Olivieri, C, V.S, M, Gao, J, Bernlohr, DA, Calebiro, D, Taylor, SS & Veglia, G 2021, 'Is disrupted nucleotide-substrate cooperativity a common trait for Cushing's syndrome driving mutations of protein kinase A?', *Journal of Molecular Biology*, vol. 433, no. 18, 167123. <http://10.1016/j.jmb.2021.167123>

The allosteric E31V mutation disrupts the nucleotide-substrate cooperativity in protein kinase A: is there a common mechanism for Cushing's syndrome driving mutations?

Caitlin Walker[1], Yingjie Wang[1,2,†], Jiali Gao[2,3], David A. Bernlohr[1], Davide Calebiro[4,5], Susan S. Taylor[6,7], and Gianluigi Veglia[1,2,*]

[1]*Department of Biochemistry, Molecular Biology, and Biophysics, University of Minnesota, Minneapolis, MN 55455, USA*

[2]*Department of Chemistry and Supercomputing Institute, University of Minnesota, Minneapolis, MN 55455, USA*

[3]*Institute of Systems and Physical Biology, Shenzhen Bay Laboratory, Shenzhen, 518055, China*

[4]*Institute of Metabolism and Systems Research, University of Birmingham, B15 2TT, Birmingham, UK*

[5]*Centre of Membrane Proteins and Receptors, University of Birmingham, B15 2TT, Birmingham, UK*

[6]*Department of Chemistry and Biochemistry, University of California at San Diego, La Jolla, CA 92093*

[7]*Department of Pharmacology, University of California at San Diego, La Jolla, CA 92093*

†Present Address: *Institute of Systems and Physical Biology, Shenzhen Bay Laboratory, Shenzhen, 518055, China*.

*Corresponding Author

Gianluigi Veglia
Department of Chemistry and Department of Biochemistry, Molecular Biology, and Biophysics,
321 Church Street SE
Minneapolis, MN 55455
Telephone: (612) 625-0758
Fax: (612) 625-5780
e-mail: vegli001@umn.edu

ABSTRACT

Somatic mutations in the *PRKACA* gene encoding the catalytic α subunit of protein kinase A (PKA-C) are responsible for cortisol-producing adrenocortical adenomas. These benign neoplasms contribute to the development of Cushing's syndrome. The majority of these mutations occur at the interface between the two lobes of PKA-C and interfere with the enzyme's ability to recognize substrates and regulatory subunits, leading to aberrant phosphorylation patterns and activation. Rarely, patients with similar phenotypes carry an allosteric mutation, E31V, located at the αA-helix's C-terminal end and adjacent to the αC-helix, a critical element in assembling the active conformation of kinases, but structurally distinct from the PKA-C interface mutations. Using a combination of solution NMR, thermodynamics, and kinetic assays, and molecular dynamics simulations, we show that the E31V allosteric mutation disrupts central communication nodes between the N- and C- lobes of the enzyme as well as the nucleotide-substrate binding cooperativity, a hallmark for kinases' substrate fidelity and regulation. For both orthosteric (L205R and W196R) and allosteric (E31V) Cushing's syndrome mutants the loss of binding cooperativity is proportional to the density of the intramolecular allosteric network. This structure-activity relationship suggests a possible common mechanism for Cushing's syndrome driving mutations in which decreased nucleotide/substrate binding cooperativity is linked to loss in substrate fidelity and dysfunctional regulation.

KEYWORDS: cAMP-dependent protein kinase A, Cushing's syndrome, allostery, cooperativity.

INTRODUCTION

Cushing's syndrome is defined by a collection of symptoms that result from prolonged exposure to high cortisol levels, with patients commonly presenting with abdominal obesity, metabolic abnormalities, and hypertension [1]. Playing a fundamental role in regulating metabolism and cell proliferation in endocrine tissues, the cAMP signaling pathway and its aberrant activation are linked to several endocrine diseases [2-4]. The role of one component of this signaling cascade, cAMP-dependent protein kinase A (PKA), in Cushing's syndrome was not appreciated until recently when somatic mutations were identified in the *PRKACA* gene encoding the catalytic α subunit of PKA (PKA-C) [5-12]. To date, a total of eight mutations have been discovered. Except for one mutation, E31V, all mutations are located near the substrate-binding cleft adjacent to the catalytic/regulatory (R) subunit interface (**Figure 1A**).

PKA is the principal intracellular effector of the second messenger, cAMP. Inactive PKA exists as a holoenzyme (R_2:C_2) containing an R-subunit dimer bound to two catalytic (C) subunits [13]. Each R-subunit contains an inhibitory sequence that occupies the active site of the enzyme. Following stimulation of adenylate cyclase, two cAMP molecules bind to each R-subunit, initiating a conformational change and releasing active PKA-C. While R-subunits are the primary intracellular regulator of PKA-C, an endogenous inhibitor (PKI) inhibits PKA-C activity within the nucleus and controls nuclear exportation [14]. Spatiotemporal regulation is controlled by various ancillary proteins such as A-kinase anchoring proteins (AKAPs) that, via interactions with R-subunits, localize PKA-C near substrates [15].

PKA-C toggles between three major conformational states: open (apo), intermediate (nucleotide-bound), and closed (nucleotide/substrate-bound) [16]. This bean-shaped enzyme consists of a conserved catalytic core comprised of two lobes. The N-lobe of the kinase is smaller and contains mostly β-sheets and the αC-helix and harboring the ATP binding site, while the C-lobe comprises mostly α-helices and contains the substrate-binding cleft [17]. In contrast to other

Ser/Thr kinases, PKA-C contains an αA-helix at its N-terminus, which anchors the N-lobe to the C-lobe and contributes to the tethering/positioning of the αC-helix. This important structural motif is recognized for its role in the activation and inactivation of protein kinases [16]. E31V is located at the C-terminus of the αA-helix and adjacent to the C-terminus of the αC-helix. While other Cushing's syndrome mutations have been shown to disrupt R-subunit/PKA-C interactions, alter the enzyme's catalytic efficiency, and/or change its substrate specificity, the mechanism of dysfunction for PKA-C^{E31V} has remained elusive [18-20].

Recently, we discovered that the most common Cushing's syndrome mutation, PKA-C^{L205R}, abrogates the nucleotide/pseudosubstrate binding cooperativity by reducing the intramolecular allostery between the small and large lobe [19]. Based on these findings, we suggested that this dysfunctional binding cooperativity and altered allostery disrupts substrate recognition and interactions with R-subunits, thereby altering canonical cAMP signaling. Despite E31V and L205R being spatially distant, our previous NMR analysis suggested they are allosterically coupled [19]. Therefore, we surmised that E31V may affect the kinase's function in a manner similar to L205R, *i.e.*, the non-conservative mutation may disrupt the allosteric network and the binding cooperativity.

To dissect this allosteric mutation's effects, we carried out solution NMR spectroscopy along with isothermal titration calorimetry (ITC), kinetic assays, and molecular dynamics (MD) simulations. We found that the E31V mutation ablates the canonical positive cooperativity, typically seen for PKA-C while maintaining the kinase's catalytic efficiency. Specifically, the E31V mutation directly affects the allosteric node that connects the αA-, αC-helix, and activation loop, thereby disrupting nucleotide-substrate binding cooperativity. Finally, by comparing PKA-C^{WT} with three drivers for Cushing's syndrome, PKA-C^{E31V}, PKA-C^{L205R}, and PKA-C^{W196R}, we found a direct

relationship between the loss of binding cooperativity and the reduction of allosteric communication within the enzyme. Altogether, our results suggest the existence of a common dysfunctional mechanism for PKA-C Cushing's mutations discovered thus far.

RESULTS

E31V mutation ablates nucleotide-substrate binding cooperativity in PKA-C. To evaluate the effects of E31V on the thermodynamics of nucleotide (ATPγN) and pseudosubstrate (PKI) binding, we used isothermal titration calorimetry (ITC) [21]. Values of ΔG, ΔH, $-T\Delta S$, K_d, and cooperativity coefficients (σ) obtained for PKA-C^{E31V} are summarized in **Table S1 and S2** [19]. We found PKA-C^{WT} and PKA-C^{E31V} have similar binding affinities for ATPγN (K_d = 83 ± 8 and 91 ± 9 μM, respectively). A 7-fold higher binding affinity is observed for PKA-C^{E31V} compared to PKA-C^{WT} when binding PKI_{5-24} to their apo forms (K_d = 2.5 ± 0.5 and 17 ± 2 μM, respectively). In contrast to PKA-C^{WT}, upon saturation with ATPγN, PKA-C^{E31V} displays a 12-fold reduction in binding affinity (K_d = 0.16 ± 0.02 and 2 ± 1 μM, respectively). As previously determined, the binding of PKI_{5-24} to PKA-C^{WT} is highly cooperative (σ = 106 ± 18); in contrast, PKA-C^{E31V} displays no cooperativity with σ = 1.3 ± 0.7. To evaluate the effects of E31V on the kinase's catalytic efficiency, we carried out steady-state coupled enzyme assays using the standard substrate, Kemptide. Despite the dramatic effects on binding cooperativity, PKA-C^{E31V} displayed only a slight increase in V_{max} and a slight decrease in $K_{M,}$ resulting in similar catalytic efficiencies (k_{cat}/K_M = 0.41 ± 0.05 and 0.46 ± 0.04 for PKA-C^{WT} and PKA-C^{E31V}, respectively; **Figure 1B** and **Table S3**). Interestingly, mutagenesis of residues adjacent to the E31 site has shown similar kinetic behavior [22].

NMR mapping of nucleotide/PKI binding response. To analyze the binding response of PKA-C^{E31V} to nucleotide and pseudosubstrate, we mapped the amide backbone fingerprint of the enzyme using [^{1}H, ^{15}N]-TROSY-HSQC experiments [23]. The amide fingerprints of the kinase in different ligated forms are displayed in **Figure S1**. The global response of the two kinases to

ligand binding was determined using CONCISE (COordiNated ChemIcal Shifts bEhavior) [24], which performs a statistical analysis on linear chemical shift trajectories of amide resonances to identify the position of each state along the conformational equilibrium, shows that nucleotide and pseudosubstrate shift the overall populations from an open state to an intermediate and fully closed state. Upon binding the nucleotide, the probability density of the amide resonances from the apo shifts toward an intermediate state, and the subsequent saturation with PKI peptide further shifts toward the fully closed state (**Figure 1C**). Globally wild-type and mutant behave similarly; however, upon binding ATPγN, PKA-C^{E31V} adopts a more open conformation compared to PKA-C^{WT} and subsequent binding of PKI shifts the probability distribution toward a more closed state.

To further confirm the changes in the global response of PKA-C induced by E31V, we mapped the chemical shift perturbations (CSP, $\Delta\delta$) of PKA-C^{E31V}. Upon binding ATPγN, PKA-C^{E31V} exhibits similar CSP patterns as wild-type (**Figure 2A,C**) with larger CSPs occurring throughout the N-lobe and in the c-terminal tail, though to a lesser extent than PKA-C^{WT}. Further analysis of the ΔCSP ($\Delta\delta_{WT}$-$\Delta\delta_{E31V}$) shows regions of positive ΔCSP confirming that upon binding ATPγN, PKA-C^{E31V} does not adopt as closed of a conformation as the wild-type kinase (**Figure S2A**). Subsequent binding of PKI to ATPγN-saturated PKA-C^{E31V} also exhibits similar CSPs compared to wild-type (**Figure 2B,D**), though to a larger extent as reflected in the negative ΔCSP values (**Figure S2B**).

Rearrangement of the allosteric network of PKA-C^{E31V} is linked to a decrease in nucleotide-substrate binding cooperativity. Since cooperativity is often manifested as structural rearrangements upon ligand binding, we further analyzed the chemical shift perturbations of PKA-C^{WT} and PKA-C^{E31V} using CHEmical Shift Covariance Analysis (CHESCA). This statistical method identifies covariant residues networks involved in a concerted response upon ligand binding and help tracing allosteric pathways [25-27]. The [^{1}H, ^{15}N]-TROSY-HSQC spectra of four forms of wild-type

and PKA-C^{E31V} (apo, ATPγN-bound, ADP-bound, and ATPγN/PKI-bound) were used for CHESCA. When we analyzed the chemical shifts changes of PKA-C^{WT}, we identified a well-organized communication network in which spatially distinct clusters of residues responding to ATP and PKI binding in a coordinated manner [19]. In contrast, we observed a dramatic reduction in the intramolecular allosteric network of PKA-C^{E31V} similar to PKA-C^{L205R}, a Cushing's syndrome mutation with significantly higher occurrence [18, 19, 28]. In particular, highly correlated groups of residues in the N-lobe of PKA-C^{E31V}, including the αA-helix (K28, W30) and αC-helix (A97), display a dramatic reduction in the number of correlations for distal regions of the kinase, including the activation loop (R190, G193, L198), αF-helix (K217, V219, G225), and C-terminal tail (E334, N340, E349) (**Figure 3**). Notably, the loss of correlations occurs in structural elements surrounding the αC-helix.

The typical CHESCA analysis gives pairwise correlations along the primary protein sequences. Therefore, we adopted the definition of structural 'communities' introduced by McClendon *et al.* [29] to obtain a three-dimensional view of the correlated structural changes. Using this analysis, we found strong correlations among the major communities in response to nucleotide and pseudosubstrate binding (**Figure 4**) [29]. In particular, ComA, ComB, and ComC show average correlation coefficients higher than 0.95, indicating that these communities respond to ligand binding in a concerted manner. Notably, there are long-range correlations between ComA, ComB, and ComC with ComE, ComF and ComF1. ComC, which encompasses the αA- and αC-helix including E31, acts as a central hub, connecting six other communities as it is centered around a critical allosteric mediator the αC-helix, which bridges both lobes of the kinase. The density of these correlations underscores the concerted response of the N- and C-lobe to ligand binding. While the E31V mutation exhibits some of the local and long-range correlations, the values of the correlation coefficients are lower. ComC and parts of the activation loop of the mutant exhibit the

most noticeable reduction in correlation to both local (ComA and ComB) and distal (ComE and ComF) communities.

MD simulations reveal altered conformational states of PKA-C^{E31V} correlated to the reduction in binding cooperativity. To determine the effects of the E31V mutation on the conformational energy landscape of nucleotide-bound PKA-C, we carried out parallel MD simulations in explicit water. We set up the simulations starting from the X-ray coordinates of PKA-C^{WT} (PDB: 4WB5 [30]) mutating E31 into a valine and removing PKI [17]. After initial equilibration, we produced an MD trajectory and analyzed the backbone flexibility of PKA-C^{E31V}. Relative to PKA-C^{WT}, we observed increased root mean squared fluctuations (RMSF) of the backbone coordinates with effects that propagate to distal domains [31], including the N-lobe, activation loop, as well as the C-terminal tail (**Figure 5A**). The most noticeable effect of the E31V mutation is the increase in the αA-helix motions, presumably due to V31 moving towards the kinase's hydrophobic interior and disrupting the cation-π interactions between W30, R93 and R190. These 'sandwiched' cation-π interactions have been shown to be partially responsible for positioning the indole ring of W30 in a conserved pocket that can be exploited to regulate kinases activity [22, 32]. As the αA-helix is displaced, the indole ring of W30 undergoes a 180° flip, maintaining only one cation-π interaction with R190 (**Figure 5B**). This motion is accompanied by the activation loop of PKA-C^{E31V} adopting a *flipped* conformation similar to the L205R mutant in which an electrostatic node between the phosphate group of pT197, the guanidinium group of R194 of the activation loop, and the side chain of E86 of the αC-helix is formed (**Figure 5C**) [19]. These new interactions cause the opening of the N-lobe and an outward tilt, involving the Gly-rich loop, αB-, and αC-helix. These motions can be inferred from the distance distributions of the conserved residues K72 and E91 residues, and the distance between the αC-helix (E86) and the activation loop (R194) (**Figure 5D**). In contrast to the stable K72-E91 salt bridge (~2.8 Å) observed for PKA-C^{WT}, the distance between K72 and E91 in PKA-C^{E31V} varies between 2.8 and 4.8 Å, sampling more frequently a conformation

223 that resembles the α*C-out* inactive state [33]. This large conformational change of the N-lobe is
224 corroborated by chemical shift changes observed for residues within the αB-helix (K76) and αC-
225 helix (Q96) (**Figure 5E**).
226 To link the MD simulations to the binding thermodynamics derived from the ITC experi-
227 ments, we computed the difference in free energy of binding ($\Delta\Delta G_{binding}$) for PKA-C^{WT} and PKA-
228 C^{E31V} using the free energy perturbation (FEP) method [34], as detailed in the thermodynamic
229 cycle shown in **Figure S3**. The ratio of the cooperativity coefficients can be expressed in terms of
230 free energy:

231 $$\frac{\sigma_{PKI}^{WT}}{\sigma_{PKI}^{E31V}} = \frac{K_{d\ Apo}^{WT} * K_{d\ Nucleotide}^{E31V}}{K_{d\ Nucleotide}^{WT} * K_{d\ Apo}^{E31V}} = \frac{K_{d\ Apo}^{WT}}{K_{d\ Apo}^{E31}} \times \frac{K_{d\ Nucleotide}^{E31V}}{K_{d\ Nucleotide}^{WT}} = e^{-\frac{\Delta\Delta G_{Nucleotide} - \Delta\Delta G_{Apo}}{RT}}$$

232 $$= e^{-\frac{\left(\Delta G_4 - \Delta G_3\right) - \left(\Delta G_2 - \Delta G_1\right)}{RT}}$$

233 Where $\frac{\sigma_{PKI}^{WT}}{\sigma_{PKI}^{E31V}}$ represents the ratio of the cooperativity coefficients for wild-type and E31V, and the
234 free energy change of a mutation in different states ΔG_1 to ΔG_4 is illustrated in **Figure S3A**. Us-
235 ing this expression for the binding of PKI to apo PKA-C^{E31V}, the FEP method calculates a free
236 energy difference between the free and bound state of -1.1 ± 0.3 kcal/mol, corresponding to a ~7-
237 fold reduction in the binding affinity of PKA-C^{E31V} for PKI . This value is in excellent agreement
238 with the experimental results (**Table S5**). On the other hand, the binding of PKI to the nucleotide-
239 bound E31V mutant resulted in a free energy perturbation of 0.3 $\pm$ 0.2 kcal/mol, indicating a
240 reduction in binding affinity. From the differences of these two values, it is possible to estimate
241 approximately a 11-fold reduction in the nucleotide/PKI binding cooperativity (**Figure S3B**), which
242 is in qualitative agreement with ITC experiments. We also calculated the change in cooperativity
243 for binding PKI first and then the nucleotide (**Figure S3C**). These calculations confirmed the re-
244 duction in cooperativity with a value that is approximately 24-fold lower for the ATP binding by

PKA-C^{E31V}, further supporting the experimentally observed loss in cooperativity for PKA-C^{E31V} (**Table S5**).

Nucleotide-substrate binding cooperativity and extent of allosteric communication are directly correlated. Both thermodynamic and NMR data show that Cushing's syndrome mutants, PKA-C^{L205R} and PKA-C^{E31V}, exhibit reduced binding cooperativity and decreased intramolecular allosteric communication. Therefore, we hypothesized that the coordinated structural changes might be correlated to the nucleotide-substrate cooperative binding response. Hence, a disruption of the allosteric network would directly affect the nucleotide-substrate binding cooperativity. To test this, we analyzed the thermodynamics and structural response of PKA-C^{W196R}, another mutant that was found in 3% of Cushing's patients [20]. This mutation is located in the activation loop and is adjacent to the T197 phosphorylation site. We repeated both ITC and NMR analysis for PKA-C^{W196R}, and similarly to PKA-C^{E31V} we found a significant attenuation in both binding cooperativity and extent of intramolecular allosteric communication (**Table S4**, **Figure S4**). From the CHESCA matrices of these three mutants and PKA-C^{WT}, we extracted the relative correlation score (see Material and Methods), which can be used to estimate the density of the intramolecular allosteric networks. We then plot the relative correlation scores versus ln(σ). We found that these parameters are linearly correlated (R^2 = 0.98, **Figure 6**). This relationship suggests that the extent of the nucleotide-substrate binding cooperativity depends on the coordinated structural changes of the two lobes of the enzyme upon nucleotide and substrate binding.

DISCUSSION

The genetic basis of adrenocortical adenomas (ACAs) has been known for the past decade, with the cAMP/PKA pathway playing a central role in adrenocortical growth steroidogenesis [3, 4]. Although multiple components of the cAMP/PKA pathway have been implicated in various endocrine disease states, it was not until recently that PKA-C was discovered to play a central role [35]. To date, eight mutations have been discovered in *PRKACA* as a rare genetic alteration in

271 cortisol-producing ACA's responsible for Cushing's syndrome [5-12]. Except for E31V, all muta-
272 tions are positioned in the substrate binding cleft or at the R/C interface, providing a justification
273 for the loss of substrate fidelity and regulation of the kinase [19, 20]. However, it has been difficult
274 to rationalize why the E31V mutant results in the same phenotype of the other orthosteric Cush-
275 ing's syndrome driving mutations. This present study shows that local conformational changes
276 caused by the E31V mutation alter key allosteric interactions that link the terminal regions of the
277 C-terminal tail, αA- and αC-helix. MD simulations revealed that the E31V mutation increases the
278 conformational dynamics within the αA-helix, causing it to dislodge from the kinase core and
279 thereby disrupting canonical cation-π interactions between W30 and R93 and R190 [36, 37].
280 These structural alterations cause the N-lobe of the kinase to swing outward adopting a more
281 open conformation, with the activation loop in a *flipped* conformation, forming a stable salt bridge
282 with the αC-helix and disrupting a critical allosteric node responsible for inter-lobe allosteric com-
283 munication and binding cooperativity [36].
284 Cooperativity is fundamental factor for macromolecular assembly and signal amplification
285 [38-40]. For PKA-C, binding cooperativity has been used to define the role of ATP as an allosteric
286 effector, able to amplify the substrate's binding affinity [41]. However, PKA-C interacts with other
287 binding partners including the R-subunits that keep its function under strict control. Notably, the
288 R-subunits recognition sequences are highly homologous to those of substrates and PKI. There-
289 fore, it is likely that the loss in nucleotide/PKI binding cooperativity we observed for these Cush-
290 ing's syndrome mutants may negatively affect the assembly of the R:C complex and the entire
291 cAMP signaling pathway.
292 In conclusion, we identified a common trait between orthosteric and allosteric mutations
293 linked to Cushing's syndrome. These mutations display a reduced binding cooperativity with a
294 concomitant loss in intramolecular allosteric communication. The effects derived by these events
295 are manifested as a loss of substrate fidelity and regulation by the R-subunit, while the catalytic

activity of these mutants remains essentially unaltered. These results may explain how these aberrant enzymes give rise to anomalous phosphoproteomic profiles [20].

MATERIALS AND METHODS

Sample Preparation. Recombinant human Cα subunit of cAMP-dependent protein kinase A cDNA (PKA-C^{WT} and PKA-C^{E31V}) was cloned into a pET-28a vector. A tobacco etch virus (TEV) cleavage site was incorporated via mutagenesis into the vector between the cDNA coding for the kinase and a thrombin cleavage site. The kinase was expressed in *Escherichia coli* BL21 (DE3) according to procedures previously published [19]. PKI (full-length) was expressed and purified according to procedures previously published [42]. Peptides (Kemptide/PKI_{5-24}) were synthesized using standard Fmoc chemistry on a CEM Liberty Blue microwave synthesizer, cleaved with Reagent K (82.5% TFA, 5% phenol, 5% thioanisole, 2.5% ethanedithiol, and 5% water) for 3 h and purified using a semipreparative Supelco C18 reverse-phase HPLC column at 3 mL/min. Molecular weight and the quantity of the peptides were verified by LC-MS and/or amino acid analysis (Texas Tech Protein Chemistry Laboratory).

ITC Measurements. ITC measurements were performed with a low-volume NanoITC (TA Instruments). PKA-C^{WT} and PKA-C^{E31V} were dialyzed into 20 mM MOPS, 90 mM KCl, 10 mM DTT, 10 mM $MgCl_2$, and 1 mM NaN_3 (pH 6.5). PKA-C concentrations for ITC measurements were between 100-110 μM as confirmed by A_{280} = 53860 $M^{-1}cm^{-1}$. All measurements with ATPγN saturated PKA-C^{WT} and PKA-C^{E31V} were performed at 2 mM ATPγN. ITC measurements were performed at 300K in triplicates. Approximately 300 μL of PKA-C was used for each experiment, and 50 μL of 2 mM ATPγN and 0.6-0.8 mM PKI in the titrant syringe. The heat of dilution of the ligand into the buffer was taken into account for all experiments and subtracted. Curves were analyzed with the NanoAnalyze software (TA Instruments) using the Wiseman Isotherm [21]:

$$\frac{d[MX]}{d[X_{tot}]} = \Delta H^{\circ} V_0 \left[\frac{1}{2} + \frac{1-\frac{1-r}{2}-R_m/2}{(R_m^2-2R_m(1-r)+(1+r)^2)^{1/2}}\right] \qquad (1)$$

where *d[MX]* is the change in total complex with respect to change in total protein concentration, *d[X_{tot}]* is dependent on *r*, the ratio of K_d with respect to the total protein concentration, and R_M, the ratio between total ligand and total protein concentration. The free energy of binding was determined using the following:

$$\Delta G = RT \ln K_d$$

where R is the universal gas constant and T is the temperature at measurement (300K). The entropic contribution to binding was calculated using the following:

$$T\Delta S = \Delta H - \Delta G.$$

Calculations for the cooperativity constant (σ) were calculated as follows:

$$\sigma = \frac{K_{d\ Apo}}{K_{d\ Nucleotide}}$$

where $K_{d\ Apo}$ is the K_d of PKI_{5-24} binding to the apoenzyme and $K_{d\ Nucleotide}$ is the K_d of PKI_{5-24} binding to the nucleotide-bound enzyme.

Enzyme Assays. Steady-state activity assays with Kemptide were performed under saturating ATP concentrations and spectrophotometrically at 298K as described by Cook et al [43]. The values of V_{max} and K_M were obtained from a nonlinear fit of the initial velocities to the Michaelis-Menten equation.

NMR Spectroscopy. Uniformly ^{15}N-labeled PKA-C^{WT} and PKA-C^{E31V} were overexpressed and purified as described above. NMR experiments were performed in 90 mM KCl, 20 mM KH_2PO_4, 10 mM dithiothreitol (DTT), 10 mM $MgCl_2$, and 1 mM NaN_3 at pH 6.5. Standard [^1H-^{15}N]-TROSY-HSQC experiments were carried out for PKA-C^{E31V} and PKA-C^{WT} on a 900-MHz Bruker Advance III spectrometer equipped with a TCI cryoprobe. Concentrations for samples were 0.2-0.3 mM as determined by A_{280} measurements, 12 mM ATPγN was added for the nucleotide-bound form, and

342 0.2-1.2 mM PKI for the ternary complex. Spectra were collected at 300K, processed using
343 NMRPipe [44], and visualized using Sparky [45].

344 All [^{1}H-^{15}N]-TROSY-HSQC experiments were acquired with 2048 (proton) and 256 (nitrogen)
345 complex points. Combined chemical shift perturbations were calculated using ^{1}H and ^{15}N chemi-
346 cal shifts according to the following:

347 $$\Delta\delta = \sqrt{(\Delta\delta H)^2 + 0.154(\Delta\delta N)^2} \quad (1)$$

348 **Chemical Shift Analyses**.

349 ***COordiNated ChemIcal Shift bEhavior (CONCISE).*** CONCISE was used to monitor chemical
350 shift trajectories and measure the change in equilibrium position using each PKA-C construct
351 (apo, ATPγN, ADP, ATPγN/PKI). This method uses principal component analysis to identify sets
352 of residues whose chemical shifts respond linearly to a conformational transition (i.e. open, inter-
353 mediate, and closed). Each residue provides a measure of the equilibrium position for each PKA-
354 C construct in the form of scores along the first principal component (PC1). To identify the resi-
355 dues whose chemical shifts follow a linear trajectory, a threshold of 3.0 for the ratio of the standard
356 deviations of PC1 over PC2 was used, and residues not exhibiting a significant chemical shift
357 were excluded based on the linewidth.

358 ***CHEmical Shift Covariance Analysis (CHESCA)***. CHESCA was used to identify and function-
359 ally characterize allosteric networks of residues eliciting concerted responses to, in this case,
360 nucleotide and pseudosubstrate. A total of four states were used to identify inter-residue correla-
361 tions: apo, ADP-bound, ATPγN-bound, and ATPγN/PKI-bound. Identification of inter-residue cor-
362 relations by CHESCA relies on agglomerative clustering (AC) and singular value decomposition
363 (SVD). Pairwise correlations between chemical shift variations experienced by different residues
364 are analyzed to identify networks of coupled residues and when plotted on a correlation matrix,
365 allows for the identification of regions that are correlated to one another. A correlation coefficient

(R_{ij}) cutoff of 0.96 was used to filter non-linear residues. Residues not exhibiting a significant chemical shift (small shifts in ppm) were excluded based on linewidth. For each residue the max change in chemical shift was calculated in both the ^{1}H (*x*) and ^{15}N (*y*) dimension ($\Delta\delta_{x,y}$). Residues were included in CHESCA analysis only if they satisfied the following: $\Delta\delta_{x,y} > ½\ \Delta v_{xA,yA} + ½\ \Delta v_{xB,yB}$, where *A* and *B* correspond to two different forms analyzed (note there is no dependence on which two forms satisfied this statement). Correlation scores were used to quantify the CHESCA correlation for each residue. Mathematically it is defined as the following: Corr. Score = number of residues where R_{ij}>0.98 / total number of R_{ij}. Community CHESCA analysis is a chemical shift based correlation map between various functional communities within the kinase. Each community is a group of residues (McClendon et al.[35]) associated with a function or regulatory mechanism. Mathematically, this community-based CHESCA analysis is a selective interpretation of CHESCA, where we evaluate a correlation score between residues in various communities as shown below. In order to represent community-based CHESCA analysis we lowered the correlation cutoff such that $R_{cutoff} > 0.8$. Suppose community A and community B has n_A and n_B number of assigned residues respectively, the correlation score between A and B is defined as,

$$R_{A,B} = \text{Number of } (R_{ij} > R_{cutoff}) / (n_A * n_B).$$

Where R_{ij} is the CHESCA correlation coefficient between residue i (belongs to community A) and residue j (belongs to community B). R_{cutoff} is the correlation value cutoff. $R_{A,B}$ can take values from 0 (no correlation between residues in A and B) to 1 (all residues in A has correlation > cutoff with all residues in B).

MD Simulations. We used the crystal structure of PKA-C^{WT} (PDB ID: 4WB5[30]) as the template. We further aligned the current structure with the full length PKA-C^{WT} and added the missing residues 1-12 at the N terminus. The protonation state of histidine residues followed our previous settings [31]. The protein was solvated in a rhombic dodecahedron solvent box with TIP3P water molecule layer extended approximately 10 Å away from the surface of the proteins. Counter ions

391 (K^+ and Cl^-) were added to ensure electrostatic neutrality corresponding to an ionic concentration
392 of ~150 mM. All covalent bonds involving a hydrogen atom of the protein were constrained with
393 the LINCS[46]algorithm. and long-range electrostatic interactions were treated with the particle-
394 mesh Ewald [47] method with a real-space cutoff of 10 Å. Parallel simulations on the apo form,
395 the binary form with one Mg^{2+} ion and one ATP, and the ternary form with two Mg^{2+} ions, one ATP
396 and one PKI_{5-24} were performed simultaneously using GROMACS 5.1.4 [48] with the
397 CHARMM36a1 force field [49]. Each system was minimized using the steepest decent algorithm
398 to remove bad contacts, and then gradually heated to 300K at a constant volume over 1 ns, using
399 harmonic restraints with a force constant 1000 kJ/(mol*Å^2) on heavy atoms of both proteins and
400 nucleotides. Over the following 12 ns of simulations at constant pressure (1 atm) and temperature
401 (300K), the restraints were gradually released. The systems were equilibrated for an additional
402 20 ns without positional restraints. The Parrinello-Rahman[50] barostat was used to keep the
403 pressure constant, while a V-rescale thermostat with a time step of 2 fs was used to keep the
404 temperature constant. Each system was simulated for 1.05 μs, with snapshots recorded every 20
405 ps.

406 **Relative change of cooperativity from free energy perturbation calculations**. The coopera-
407 tivity can be defined for both nucleotide and pseudosubstrate PKI, respectively. For nucleotide,
408 the change of cooperativity upon mutation can be rewritten as the difference in ΔΔG between
409 the apo and the PKI-bound state, as shown in the following equation and illustrated in **Figure**
410 **S3**:

411 $$\frac{\sigma^{WT}_{Nucleotide}}{\sigma^{E31V}_{Nucleotide}} = \frac{K^{WT}_{d\ Apo} * K^{E31V}_{d\ PKI}}{K^{WT}_{d\ PKI} * K^{E31V}_{d\ Apo}} = \frac{K^{WT}_{d\ Apo}}{K^{E31V}_{d\ Apo}} \times \frac{K^{E31V}_{d\ PKI}}{K^{WT}_{d\ PKI}} = e^{-\frac{(\Delta G_1 - \Delta G_3) + (\Delta G_4 - \Delta G_2)}{RT}}$$

412 The free energies ΔG due to amino acid mutations were determined following a protocol based
413 on the Bennett acceptance ratio (BAR) implemented in the GROMACS and PMX [34]. To avoid
414 the artifacts by introducing a charged mutation, the double-system/single-box setup was used.

The procedure employs dual protein topologies that include both residues of the wild-type ($\lambda = 0$) and the mutant protein ($\lambda = 1$) coupled by the progressing variable λ. Of course, both the complex and unbound structures were used to obtain the change in binding free energies using standard thermodynamic cycle approach. Single-site mutations were performed based on the well-equilibrated structure of PKA-C^{WT} from simulations. The computational details are identical to those detailed above, except that after 40 ns of equilibration of both initial and final states for each mutation, 200 additional trajectories, each lasting 100 ps, were initiated from the last 20 ns simulations both in the forward and in the backward transformations to accumulate statistical averages and fluctuations.

ACKNOWLEDGMENTS

This work was supported by the National Institutes of Health, GM100310 (G.V.), S10 OD021536 (G.V.) and GM046736 (J.G), and the American Heart Association, 20PRE35120253 (C.W). NMR experiments were carried out at the Minnesota NMR Center and MD calculations at the Minnesota Supercomputing Institute.

AUTHOR CONTRIBUTIONS

C.W. collected and analyzed activity assay, NMR, and ITC data and contributed to the writing of the manuscript. Y.W. carried out and analyzed MD simulations, with J.G. directing and assisting with analysis of the MD simulations. D.C, D.A.B and S.S.T contributed to critical analysis of the data and writing of the manuscript. G.V. conceived and directed the project, along with assisting with data analysis and writing the manuscript.

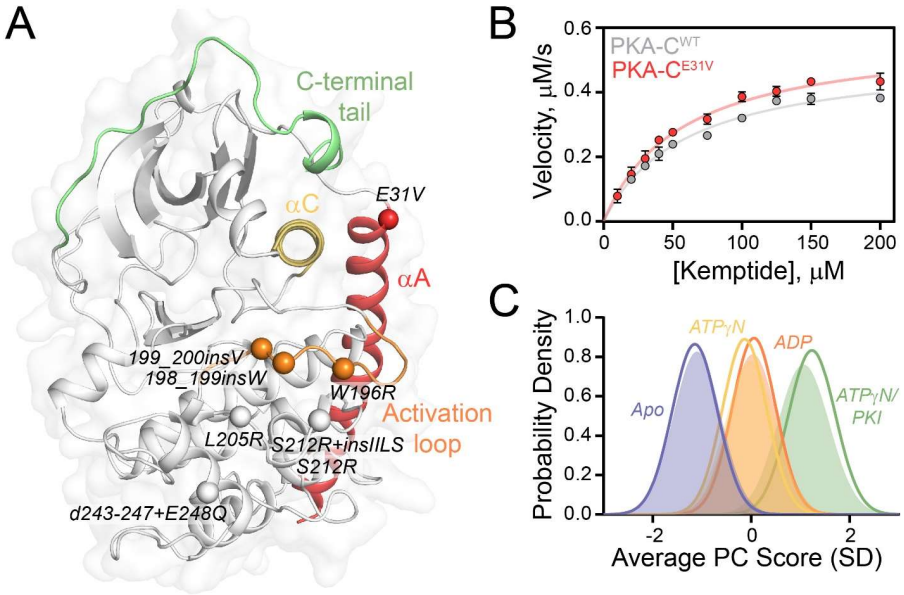

Figure 1. Structural and kinetic characterization of PKA-C^{E31V}. (**A**) Structure of PKA-C bound to endogenous inhibitor, PKI (PDB: 1ATP) highlighting important structural elements and locations of Cushing's syndrome mutations in relation to E31V. (**B**) Steady state phosphorylation kinetics of PKA-C^{E31V} with Kemptide. (**C**) CONCISE analysis on the apo, ATPγN-, ADP- and ATPγN/PKI-bound forms of PKA-C^{WT} (opaque gaussian) and PKA-C^{E31V} (outlined gaussian).

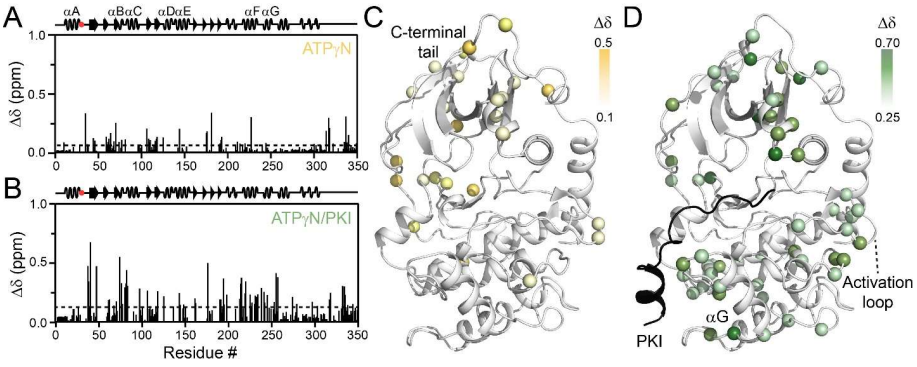

Figure 2. Chemical shift perturbation of PKA-C^{E31V}. Chemical shift perturbation (CSP) of amide fingerprint of PKA-C^{E31V} upon binding (**A**) ATPγN and subsequent binding of (**B**) PKI. The average CSP is shown as a dashed line. CSPs of PKA-C^{E31V} amide resonances mapped onto the structure (PDB: 1ATP).

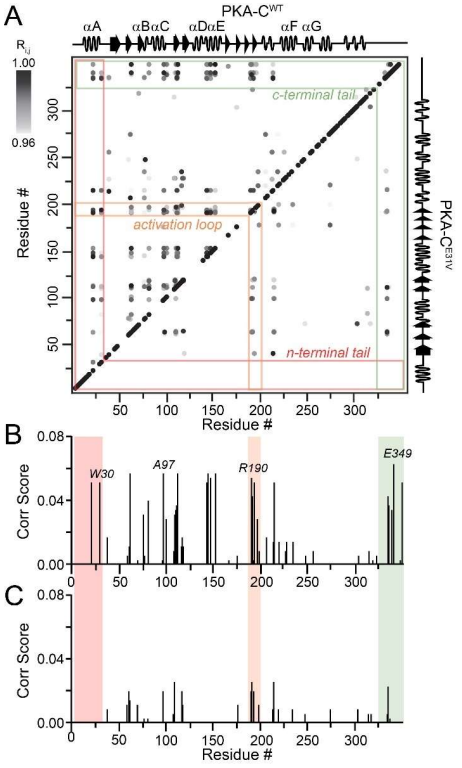

451

452 **Figure 3. The reduction in binding cooperativity corresponds to a decrease of intramolec-**
453 **ular allosteric connectivities.** (**A**) CHESCA correlation matrix of PKA-C^{WT} (top diagonal) and
454 PKA-C^{E31V} (bottom diagonal) upon binding PKI highlighting the notable reductions in correlations
455 within the n-terminal tail (red), activation loop (orange), and c-terminal tail (green). Only correla-
456 tions with R_{ij}> 0.98 are shown. Plot of correlation score vs. residue for (**B**) PKA-C^{WT} and (**C**) PKA-
457 C^{E31V} emphasizing the residues that show the largest reductions in correlation score that make
458 contacts with the αC-helix. See material and methods for the calculation of correlation scores.

459

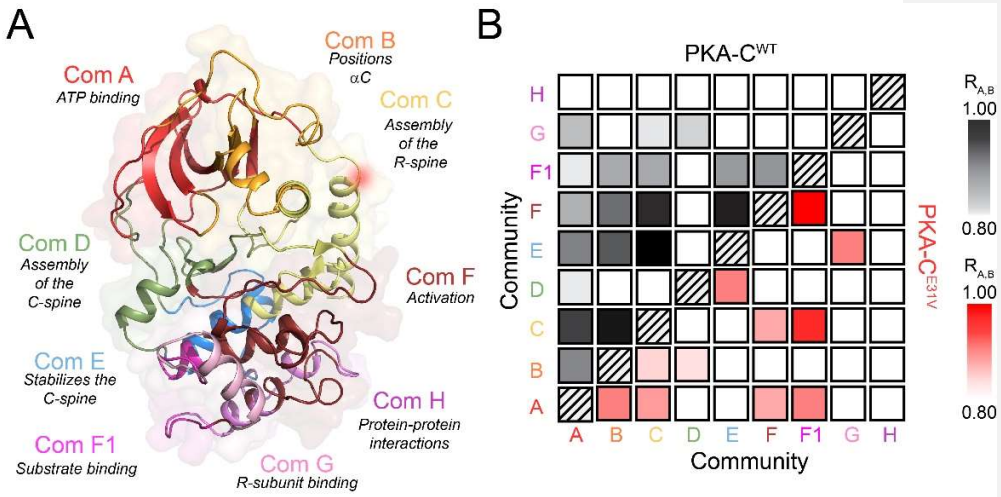

460

461 **Figure 4. NMR map of the structural responses to nucleotide and pseudo-substrate bind-**
462 **ing for wild-type and E31V mutants.** (**A**) Community map of PKA-C highlighting func-
463 tional/regulatory role of each community as defined by [29]. (**B**) Community CHESCA analysis
464 of PKA-C^{WT} (top diagonal, black) and PKA-C^{E31V} (bottom diagonal, red). Only correlations with
465 $R_{A,B}$ > 0.8 are shown.

466

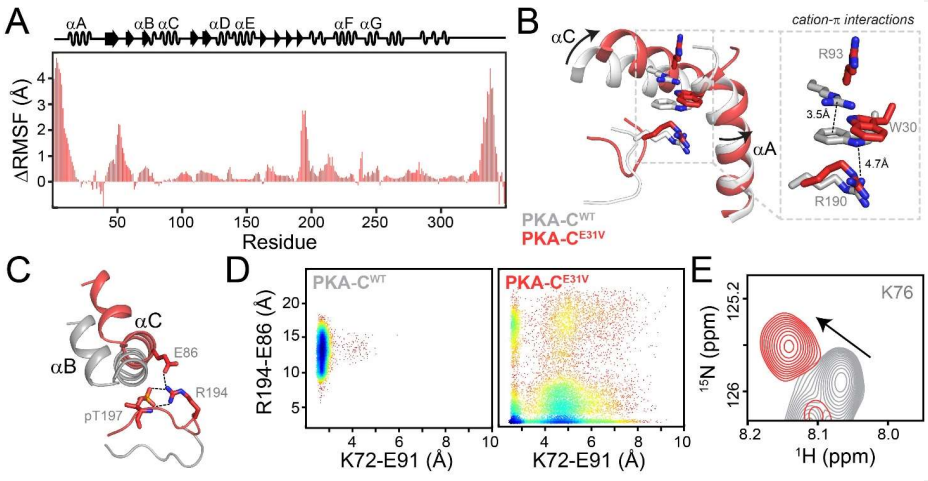

Figure 5. Comparison of MD simulations of PKA^{WT} and PKA-C^{E31V}. (**A**) Changes in the root mean square fluctuations (ΔRMSF) of PKA-C^{E31V} in the nucleotide-bound form over 1.0 μs of simulation. (**B**) Overlay of PKA-C^{WT} (PDB: 1ATP; gray) and PKA-C^{E31V} (from MD simulations; hot pink) showing the structural rearrangements of the αA- and αC-helices caused by the E31V mutation. The inset shows the cation-π stacking interactions altered in response to the mutation. (**C**) Overlay of PKA-C^{WT} (PDB: 1ATP; gray) and PKA-C^{E31V} (from MD simulations; hot pink) showing the upward movement of the αB- and αC-helices and the rearrangements of the electrostatic interactions between the activation loop and the αC-helix. (**D**) Distinct conformational dynamics of the αC-helix in PKA-C^{WT} and PKA-C^{E31V}, as characterized by the two key salt bridges K72-E91 and E86-R194. (**E**) Portion of the [^{1}H, ^{15}N]-TROSY-HSQC spectra showing the backbone amide chemical shift changes of K76 (located in αB-helix) in the PKA-C^{E31V}.

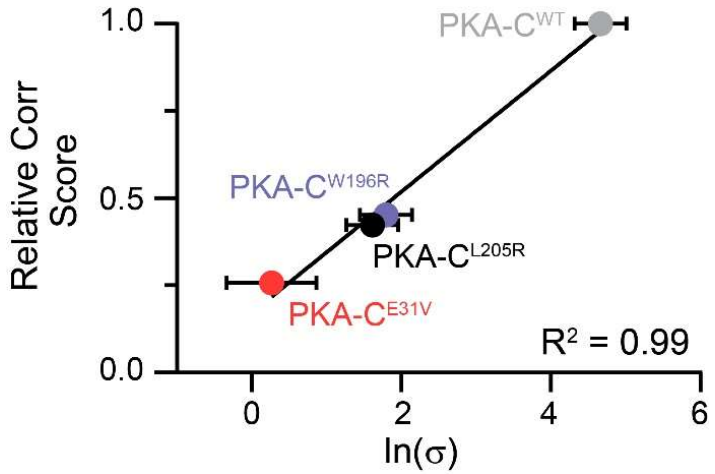

481

482 **Figure 6. Relationship between coordinated structural changes identified by CHESCA and**

483 **the nucleotide-substrate binding cooperativity (σ) determined by ITC measurements.**

484

Supplementary Information

The allosteric E31V mutation disrupts the nucleotide-substrate cooperativity in protein kinase A: is there a common mechanism for Cushing's syndrome driving mutations?

Caitlin Walker[1], Yingjie Wang[1,2,†], Jiali Gao[2,3], David A. Bernlohr[1], Davide Calebiro[4,5], Susan S. Taylor[6,7], and Gianluigi Veglia[1,2,*]

[1]*Department of Biochemistry, Molecular Biology, and Biophysics, University of Minnesota, Minneapolis, MN 55455, USA*

[2]*Department of Chemistry and Supercomputing Institute, University of Minnesota, Minneapolis, MN 55455, USA*

[3]*Institute of Systems and Physical Biology, Shenzhen Bay Laboratory, Shenzhen, 518055, China*

[4]*Institute of Metabolism and Systems Research, University of Birmingham, B15 2TT, Birmingham, UK*

[5]*Centre of Membrane Proteins and Receptors, University of Birmingham, B15 2TT, Birmingham, UK*

[6]*Department of Chemistry and Biochemistry, University of California at San Diego, La Jolla, CA 92093*

[7]*Department of Pharmacology, University of California at San Diego, La Jolla, CA 92093*

†Present Address: *Institute of Systems and Physical Biology, Shenzhen Bay Laboratory, Shenzhen, 518055, China*.

*Corresponding Author

Gianluigi Veglia
Department of Chemistry and Department of Biochemistry, Molecular Biology, and Biophysics,
321 Church Street SE
Minneapolis, MN 55455
Telephone: (612) 625-0758
Fax: (612) 625-5780
e-mail: vegli001@umn.edu

Table of Contents:

550 **Table S1. Changes in enthalpy, entropy, free energy, and dissociation constant for the**
551 **binding of nucleotide to PKA-C^{WT} and PKA-C^{E31V}.** All errors were calculated using triplicate
552 measurements. Asterisk indicates data that has been previously published [19].

	K_d (μM)	ΔG (kcal/mol)	ΔH (kcal/mol)	-TΔS (kcal/mol)
*PKA-C^{WT}	83 ± 8	-5.61 ± 0.06	-3.6 ± 0.1	- 2.0 ± 0.1
PKA-C^{E31V}	91 ± 9	-5.56 ± 0.06	-3.7 ± 0.2	-1.9 ± 0.2

553

Table S2. **Changes in enthalpy, entropy, free energy, and dissociation constant for the binding of PKI_{5-24} to apo and nucleotide-saturated PKA-C^{WT} and PKA-C^{E31V}.** Errors in ΔG, ΔH, -TΔS, and K_d were calculated using triplicate measurements. Errors in σ were propagated from error in K_d. Asterisk indicates data that has been previously published [19].

Apo forms

	K_d (μM)	ΔG (kcal/mol)	ΔH (kcal/mol)	-TΔS (kcal/mol)
*PKA-C^{WT}	17 ± 2	-6.57 ± 0.08	-10.8 ± 0.5	4.2 ± 0.5
PKA-C^{E31V}	2.5 ± 0.5	-7.7 ± 0.1	-19.8 ± 0.4	12.1 ± 0.5

ATPγN saturated forms

	K_d (μM)	ΔG (kcal/mol)	ΔH (kcal/mol)	-TΔS (kcal/mol)	σ
*PKA-C^{WT}	0.16 ± 0.02	-9.33 ± 0.07	-13.9 ± 0.5	4.6 ± 0.4	106 ± 18
PKA-C^{E31V}	2 ± 1	-7.9 ± 0.3	-17 ± 1	9 ± 1	1.3 ± 0.7

Table S3. Kinetic parameters of Kemptide phosphorylation by PKA-C^{WT} and PKA-C^{E31V}. Values for K_m and k_{cat} were obtained from a non-linear least squares analysis of the concentration-dependent initial phosphorylation rates using a standard coupled enzyme activity assay. Error in k_{cat}/K_M was propagated from error in K_M and k_{cat}.

	PKA-C^{WT}	PKA-C^{E31V}
V_{max} (μM/sec)	0.52 ± 0.02	0.58 ± 0.02
K_M (μM)	59 ± 7	56 ± 5
k_{cat} (s^{-1})	24 ± 1	26 ± 1
k_{cat}/K_M	0.41 ± 0.05	0.46 ± 0.04

Table S4. Changes in enthalpy, entropy, free energy, and dissociation constant for the binding of PKI_{5-24} to apo and nucleotide-saturated PKA-C^{L205R} and PKA-C^{W196R}. Errors in ΔG, ΔH, -TΔS, and K_d were calculated using triplicate measurements. Errors in σ were propagated from error in K_d. Asterisk indicates data that has been previously published [19].

Apo forms

	K_d (μM)	ΔG (kcal/mol)	ΔH (kcal/mol)	-TΔS (kcal/mol)
*PKA-C^{L205R}	61 ± 5	-5.79 ± 0.04	-9.7 ± 0.1	3.9 ± 0.1
PKA-C^{W196R}	5 ± 2	-7.3 ± 0.2	-21.1 ± 0.8	13.8 ± 0.5

ATPγN saturated forms

	K_d (μM)	ΔG (kcal/mol)	ΔH (kcal/mol)	-TΔS (kcal/mol)	σ
*PKA-C^{L205R}	10 ± 3	-6.9 ± 0.2	-8.8 ± 0.8	1.9 ± 0.6	6 ± 2
PKA-C^{W196R}	0.95 ± 0.05	-8.28 ± 0.03	-19.2 ± 0.5	10.9 ± 0.5	5 ± 2

Table S5. Changes in relative binding free energy, ΔΔG, and cooperativity from PKA-C^{WT} to PKA-C^{31V} for the binding of PKI_{5-24} and the binding of ATP in the apo and binary states.

	$\Delta\Delta G_{apo}$ (kcal/mol)	$\Delta\Delta G_{binary}$ (kcal/mol)	Reduction in σ
PKI_{5-24} binding	-1.1 ± 0.3	0.3 ± 0.2	11 ± 5
ATP binding	-0.8 ± 0.2	1.1 ± 0.3	24 ± 9

Commented [GV1]: Need to include W196R

Figure S1. [^{1}H, ^{15}N]-TROSY-HSQC spectra for PKA-C^{WT} and PKA-C^{E31V} in the apo, ATPγN-, ADP-, and ATPγN/PKI-bound forms.

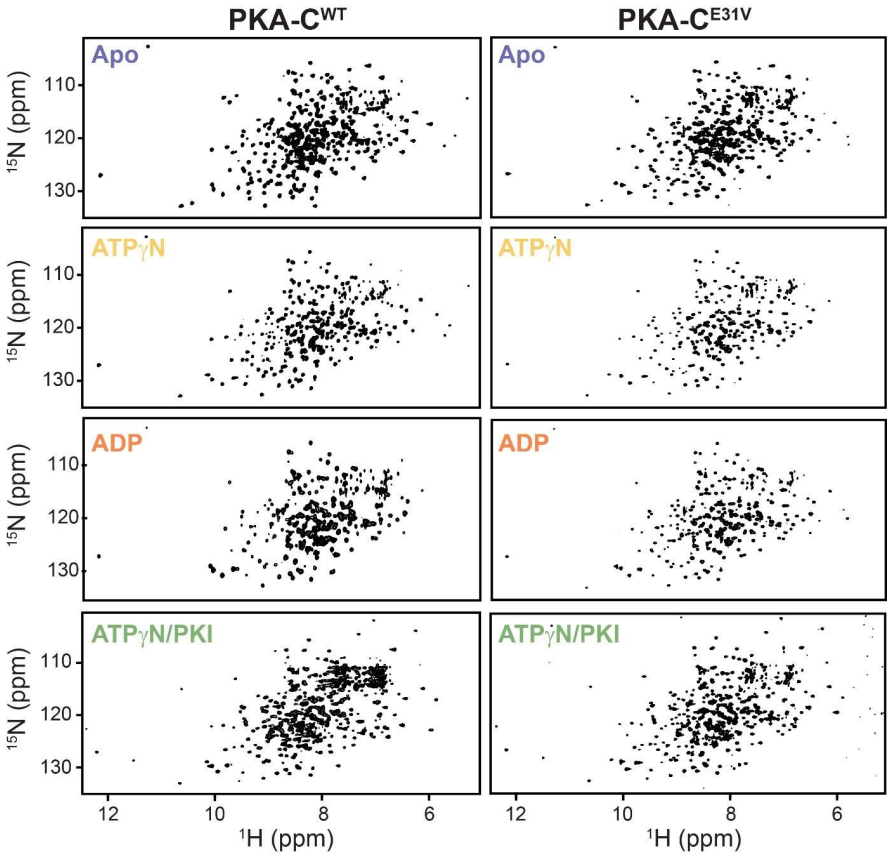

Figure S2. Change in chemical shift perturbation between PKA-C^{WT} and PKA-C^{E31V}.

Change in CSP ($\Delta\delta_{WT}$-$\Delta\delta_{E31V}$) upon binding (**A**) ATPγN. and subsequent binding of (**B**) PKI.

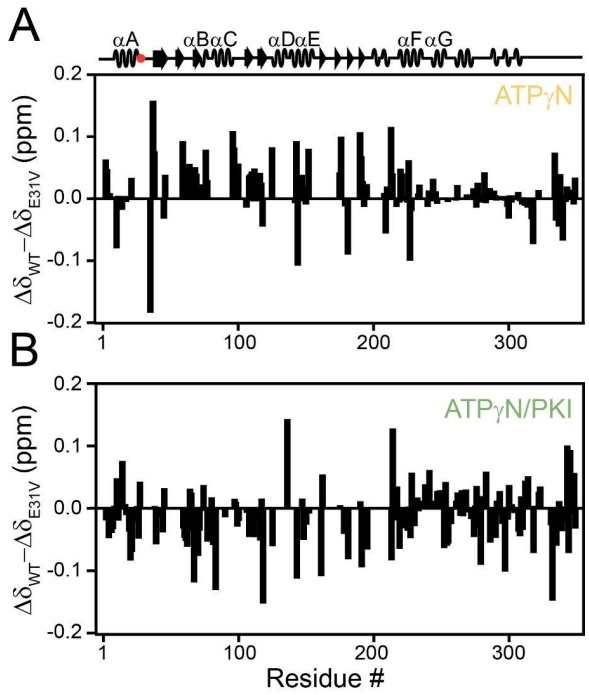

Figure S3. Thermodynamic cycle linking the free energy perturbation (FEP) calculation to ratio of K_d and σ. (**A**). Alchemical transition steps that determine the relative change of binding free energy. The change in PKI-binding to the apo state upon mutation can either be obtained from the experimental ratio $\frac{K_{d\ Apo}^{E31V}}{K_{d\ Apo}^{WT}}$, or be computed from the difference between the two alchemical transition ΔG_2-ΔG_1. (**B**). Computational scheme used to determine the ratio of the cooperativity coefficients (σ). $\Delta\Delta G_{21}$ is directly computed by grouping the two alchemical transitions in the same simulation box with forward transition of WT -> E31V, along with the reverse transition of E31V/PKI_{5-24} -> WT/PKI_{5-24}. The same computational scheme was used to determine $\Delta\Delta G_{43}$. The ratio of σ was derived from the difference between $\Delta\Delta G_{21}$ and $\Delta\Delta G_{43}$. (**C**). Computational scheme used to determine the ratio of the cooperativity coefficients σ' calculating $\Delta\Delta G_{13}$ and $\Delta\Delta G_{42}$, respectively.

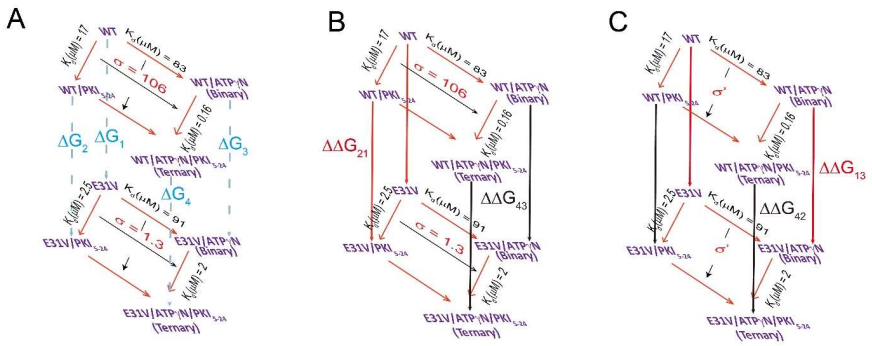

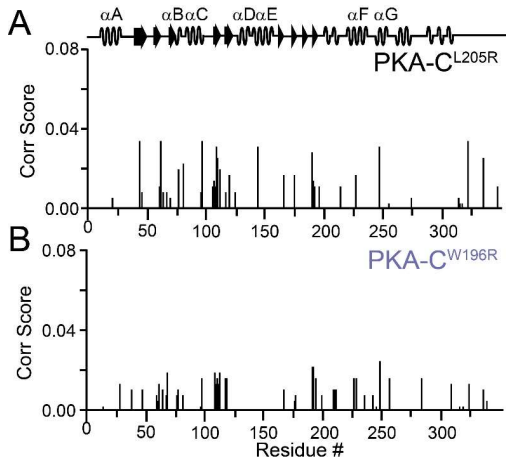

Figure S4.

Commented [GV2]: Need to complete this figure legend

1. Lacroix, A., Feelders, R. A., Stratakis, C. A. & Nieman, L. K. (2015). Cushing's syndrome. *Lancet* **386**, 913-27.
2. Lodish, M. & Stratakis, C. A. (2016). A genetic and molecular update on adrenocortical causes of Cushing syndrome. *Nat Rev Endocrinol* **12**, 255-62.
3. Calebiro, D., Di Dalmazi, G., Bathon, K., Ronchi, C. L. & Beuschlein, F. (2015). cAMP signaling in cortisol-producing adrenal adenoma. *European Journal of Endocrinology* **173**, M99-M106.
4. Calebiro, D., Bathon, K. & Weigand, I. (2017). Mechanisms of Aberrant PKA Activation by Cα Subunit Mutations. *Horm Metab Res* **49**, 307-314.
5. Goh, G., Scholl, U. I., Healy, J. M., Choi, M., Prasad, M. L., Nelson-Williams, C., Kunstman, J. W., Korah, R., Suttorp, A. C., Dietrich, D., Haase, M., Willenberg, H. S., Stålberg, P., Hellman, P., Akerström, G., Björklund, P., Carling, T. & Lifton, R. P. (2014). Recurrent activating mutation in PRKACA in cortisol-producing adrenal tumors. *Nat Genet* **46**, 613-7.
6. Cao, Y., He, M., Gao, Z., Peng, Y., Li, Y., Li, L., Zhou, W., Li, X., Zhong, X., Lei, Y., Su, T., Wang, H., Jiang, Y., Yang, L., Wei, W., Yang, X., Jiang, X., Liu, L., He, J., Ye, J., Wei, Q., Li, Y., Wang, W., Wang, J. & Ning, G. (2014). Activating hotspot L205R mutation in PRKACA and adrenal Cushing’s syndrome. *Science* **344**, 913-917.
7. Di Dalmazi, G., Kisker, C., Calebiro, D., Mannelli, M., Canu, L., Arnaldi, G., Quinkler, M., Rayes, N., Tabarin, A., Laure Jullié, M., Mantero, F., Rubin, B., Waldmann, J., Bartsch, D. K., Pasquali, R., Lohse, M., Allolio, B., Fassnacht, M., Beuschlein, F. & Reincke, M. (2014). Novel somatic mutations in the catalytic subunit of the protein kinase A as a cause of adrenal Cushing's syndrome: a European multicentric study. *J Clin Endocrinol Metab* **99**, E2093-100.
8. Beuschlein, F., Fassnacht, M., Assié, G., Calebiro, D., Stratakis, C. A., Osswald, A., Ronchi, C. L., Wieland, T., Sbiera, S., Faucz, F. R., Schaak, K., Schmittfull, A., Schwarzmayr, T., Barreau, O., Vezzosi, D., Rizk-Rabin, M., Zabel, U., Szarek, E., Salpea, P., Forlino, A., Vetro, A., Zuffardi, O., Kisker, C., Diener, S., Meitinger, T., Lohse, M. J., Reincke, M., Bertherat, J., Strom, T. M. & Allolio, B. (2014). Constitutive Activation of PKA Catalytic Subunit in Adrenal Cushing's Syndrome. *New England Journal of Medicine* **370**, 1019-1028.
9. Ronchi, C. L., Di Dalmazi, G., Faillot, S., Sbiera, S., Assié, G., Weigand, I., Calebiro, D., Schwarzmayr, T., Appenzeller, S., Rubin, B., Waldmann, J., Scaroni, C., Bartsch, D. K., Mantero, F., Mannelli, M., Kastelan, D., Chiodini, I., Bertherat, J., Reincke, M., Strom, T. M., Fassnacht, M., Beuschlein, F. & Tumors, o. b. o. t. E. N. f. t. S. o. A. (2016). Genetic Landscape of Sporadic Unilateral Adrenocortical Adenomas Without PRKACA p.Leu206Arg Mutation. *The Journal of Clinical Endocrinology & Metabolism* **101**, 3526-3538.
10. Sato, Y., Maekawa, S., Ishii, R., Sanada, M., Morikawa, T., Shiraishi, Y., Yoshida, K., Nagata, Y., Sato-Otsubo, A., Yoshizato, T., Suzuki, H., Shiozawa, Y., Kataoka, K., Kon, A., Aoki, K., Chiba, K., Tanaka, H., Kume, H., Miyano, S., Fukayama, M., Nureki, O., Homma, Y. & Ogawa, S. (2014). Recurrent somatic mutations underlie corticotropin-independent Cushing's syndrome. *Science* **344**, 917-20.
11. Thiel, A., Reis, A. C., Haase, M., Goh, G., Schott, M., Willenberg, H. S. & Scholl, U. I. (2015). PRKACA mutations in cortisol-producing adenomas and adrenal hyperplasia: a single-center study of 60 cases. *Eur J Endocrinol* **172**, 677-85.
12. Nakajima, Y., Okamura, T., Gohko, T., Satoh, T., Hashimoto, K., Shibusawa, N., Ozawa, A., Ishii, S., Tomaru, T., Horiguchi, K., Okada, S., Takata, D., Rokutanda, N., Horiguchi,

J., Tsushima, Y., Oyama, T., Takeyoshi, I. & Yamada, M. (2014). Somatic mutations of the catalytic subunit of cyclic AMP-dependent protein kinase (PRKACA) gene in Japanese patients with several adrenal adenomas secreting cortisol [Rapid Communication]. *Endocr J* **61**, 825-32.

13. Taylor, S. S., Ilouz, R., Zhang, P. & Kornev, A. P. (2012). Assembly of allosteric macromolecular switches: lessons from PKA. *Nature Reviews Molecular Cell Biology* **13**, 646.
14. Taylor, S. S., Ilouz, R., Zhang, P. & Kornev, A. P. (2012). Assembly of allosteric macromolecular switches: lessons from PKA. *Nature reviews. Molecular cell biology* **13**, 646-58.
15. Langeberg, L. K. & Scott, J. D. (2015). Signalling scaffolds and local organization of cellular behaviour. *Nature Reviews Molecular Cell Biology* **16**, 232-244.
16. Johnson, D. A., Akamine, P., Radzio-Andzelm, E. & Taylor, S. S. (2001). Dynamics of cAMP-Dependent Protein Kinase. *Chemical Reviews* **101**, 2243-2270.
17. Knighton, D. R., Zheng, J. H., Ten Eyck, L. F., Ashford, V. A., Xuong, N. H., Taylor, S. S. & Sowadski, J. M. (1991). Crystal structure of the catalytic subunit of cyclic adenosine monophosphate-dependent protein kinase. *Science* **253**, 407-14.
18. Calebiro, D., Hannawacker, A., Lyga, S., Bathon, K., Zabel, U., Ronchi, C., Beuschlein, F., Reincke, M., Lorenz, K., Allolio, B., Kisker, C., Fassnacht, M. & Lohse, M. J. (2014). PKA catalytic subunit mutations in adrenocortical Cushing's adenoma impair association with the regulatory subunit. *Nature Communications* **5**, 5680.
19. Walker, C., Wang, Y., Olivieri, C., Karamafrooz, A., Casby, J., Bathon, K., Calebiro, D., Gao, J., Bernlohr, D. A., Taylor, S. S. & Veglia, G. (2019). Cushing's syndrome driver mutation disrupts protein kinase A allosteric network, altering both regulation and substrate specificity. *Science Advances* **5**, eaaw9298.
20. Bathon, K., Weigand, I., Vanselow, J. T., Ronchi, C. L., Sbiera, S., Schlosser, A., Fassnacht, M. & Calebiro, D. (2019). Alterations in Protein Kinase A Substrate Specificity as a Potential Cause of Cushing Syndrome. *Endocrinology* **160**, 447-459.
21. Wiseman, T., Williston, S., Brandts, J. F. & Lin, L.-N. (1989). Rapid measurement of binding constants and heats of binding using a new titration calorimeter. *Analytical Biochemistry* **179**, 131-137.
22. Herberg, F. W., Zimmermann, B., Mcglone, M. & Taylor, S. S. (1997). Importance of the A-helix of the catalytic subunit of cAMP-dependent protein kinase for stability and for orienting subdomains at the cleft interface. *Protein Science* **6**, 569-579.
23. Pervushin, K., Riek, R., Wider, G. & Wüthrich, K. (1997). Attenuated T2 relaxation by mutual cancellation of dipole–dipole coupling and chemical shift anisotropy indicates an avenue to NMR structures of very large biological macromolecules in solution. *Proceedings of the National Academy of Sciences* **94**, 12366-12371.
24. Cembran, A., Kim, J., Gao, J. & Veglia, G. (2014). NMR mapping of protein conformational landscapes using coordinated behavior of chemical shifts upon ligand binding. *Physical Chemistry Chemical Physics* **16**, 6508-6518.
25. Selvaratnam, R., Chowdhury, S., VanSchouwen, B. & Melacini, G. (2011). Mapping allostery through the covariance analysis of NMR chemical shifts. *Proceedings of the National Academy of Sciences* **108**, 6133-6138.
26. Boulton, S., Akimoto, M., Selvaratnam, R., Bashiri, A. & Melacini, G. (2014). A Tool Set to Map Allosteric Networks through the NMR Chemical Shift Covariance Analysis. *Scientific Reports* **4**, 7306.
27. Byun, J. A. & Melacini, G. (2018). NMR methods to dissect the molecular mechanisms of disease-related mutations (DRMs): Understanding how DRMs remodel functional free energy landscapes. *Methods* **148**, 19-27.

28. Di Dalmazi, G., Kisker, C., Calebiro, D., Mannelli, M., Canu, L., Arnaldi, G., Quinkler, M., Rayes, N., Tabarin, A., Laure Jullié, M., Mantero, F., Rubin, B., Waldmann, J., Bartsch, D. K., Pasquali, R., Lohse, M., Allolio, B., Fassnacht, M., Beuschlein, F. & Reincke, M. (2014). Novel somatic mutations in the catalytic subunit of the protein kinase A as a cause of adrenal Cushing's syndrome: a European multicentric study. *The Journal of clinical endocrinology and metabolism* **99**, E2093-100.
29. McClendon, C. L., Kornev, A. P., Gilson, M. K. & Taylor, S. S. (2014). Dynamic architecture of a protein kinase. *Proceedings of the National Academy of Sciences of the United States of America* **111**, E4623-31.
30. Cheung, J., Ginter, C., Cassidy, M., Franklin, M. C., Rudolph, M. J., Robine, N., Darnell, R. B. & Hendrickson, W. A. (2015). Structural insights into mis-regulation of protein kinase A in human tumors. *Proceedings of the National Academy of Sciences of the United States of America* **112**, 1374-9.
31. Masterson, L. R., Shi, L., Metcalfe, E., Gao, J., Taylor, S. S. & Veglia, G. (2011). Dynamically committed, uncommitted, and quenched states encoded in protein kinase A revealed by NMR spectroscopy. *Proceedings of the National Academy of Sciences of the United States of America* **108**, 6969-74.
32. Thompson, E. E., Kornev, A. P., Kannan, N., Kim, C., Ten Eyck, L. F. & Taylor, S. S. (2009). Comparative surface geometry of the protein kinase family. *Protein Sci* **18**, 2016-26.
33. Jura, N., Zhang, X., Endres, Nicholas F., Seeliger, Markus A., Schindler, T. & Kuriyan, J. (2011). Catalytic Control in the EGF Receptor and Its Connection to General Kinase Regulatory Mechanisms. *Molecular Cell* **42**, 9-22.
34. Gapsys, V., Michielssens, S., Seeliger, D. & de Groot, B. L. (2015). pmx: Automated protein structure and topology generation for alchemical perturbations. *Journal of Computational Chemistry* **36**, 348-354.
35. Stratakis, C. A. (2018). Cyclic AMP-dependent protein kinase catalytic subunit A (PRKACA): the expected, the unexpected, and what might be next. *J Pathol* **244**, 257-259.
36. Taylor, S. S. & Kornev, A. P. (2011). Protein kinases: evolution of dynamic regulatory proteins. *Trends in Biochemical Sciences* **36**, 65-77.
37. Cembran, A., Masterson, L. R., McClendon, C. L., Taylor, S. S., Gao, J. & Veglia, G. (2012). Conformational equilibrium of N-myristoylated cAMP-dependent protein kinase A by molecular dynamics simulations. *Biochemistry* **51**, 10186-96.
38. Williamson, J. R. (2008). Cooperativity in macromolecular assembly. *Nature Chemical Biology* **4**, 458-465.
39. Wu, H. (2013). Higher-order assemblies in a new paradigm of signal transduction. *Cell* **153**, 287-92.
40. Tsai, C. J., Del Sol, A. & Nussinov, R. (2009). Protein allostery, signal transmission and dynamics: a classification scheme of allosteric mechanisms. *Mol Biosyst* **5**, 207-16.
41. Masterson, L. R., Mascioni, A., Traaseth, N. J., Taylor, S. S. & Veglia, G. (2008). Allosteric cooperativity in protein kinase A. *Proc Natl Acad Sci U S A* **105**, 506-11.
42. Olivieri, C., Wang, Y., Li, G. C., V S, M., Kim, J., Stultz, B. R., Neibergall, M., Porcelli, F., Muretta, J. M., Thomas, D. D. T., Gao, J., Blumenthal, D. K., Taylor, S. S. & Veglia, G. (2020). Multi-state recognition pathway of the intrinsically disordered protein kinase inhibitor by protein kinase A. *eLife* **9**, e55607.
43. Cook, P. F., Neville, M. E., Vrana, K. E., Hartl, F. T. & Roskoski, R. (1982). Adenosine cyclic 3',5'-monophosphate dependent protein kinase: kinetic mechanism for the bovine skeletal muscle catalytic subunit. *Biochemistry* **21**, 5794-5799.

44. Delaglio, F., Grzesiek, S., Vuister, G., Zhu, G., Pfeifer, J. & Bax, A. (1995). NMRPipe: A multidimensional spectral processing system based on UNIX pipes. *Journal of Biomolecular NMR* **6**.
45. Lee, W., Tonelli, M. & Markley, J. L. (2015). NMRFAM-SPARKY: enhanced software for biomolecular NMR spectroscopy. *Bioinformatics* **31**, 1325-1327.
46. Hess, B., Bekker, H., Berendsen, H. J. C. & Fraaije, J. G. E. M. (1997). LINCS: A linear constraint solver for molecular simulations. *Journal of Computational Chemistry* **18**, 1463-1472.
47. Darden, T., York, D. & Pedersen, L. (1993). Particle mesh Ewald: An N·log(N) method for Ewald sums in large systems. *The Journal of Chemical Physics* **98**, 10089.
48. Hess, B., Kutzner, C., van der Spoel, D. & Lindahl, E. (2008). GROMACS 4: Algorithms for Highly Efficient, Load-Balanced, and Scalable Molecular Simulation. *Journal of Chemical Theory and Computation* **4**, 435-447.
49. Best, R. B., Zhu, X., Shim, J., Lopes, P. E. M., Mittal, J., Feig, M. & Mackerell, A. D. (2012). Optimization of the additive CHARMM all-atom protein force field targeting improved sampling of the backbone φ, ψ and side-chain χ(1) and χ(2) dihedral angles. *Journal of chemical theory and computation* **8**, 3257-3273.
50. Parrinello, M. & Rahman, A. (1980). Crystal Structure and Pair Potentials: A Molecular-Dynamics Study. *Physical Review Letters* **45**, 1196-1199.